Role of protein frame and solvent for the redox properties of azurin from *Pseudomonas aeruginosa*

Michele Cascella*, Alessandra Magistrato†, Ivano Tavernelli*, Paolo Carloni†, and Ursula Rothlisberger*§

*Ecole Polytechnique Fédérale de Lausanne, Laboratory of Computational Chemistry and Biochemistry, 1015 Lausanne, Switzerland; and †Consiglio Nazionale delle Ricerche–National Institute for the Physics of Matter–Democritos National Simulation Center and International School for Advanced Studies, Via Beirut 2–4, 34014 Trieste, Italy

Edited by Harry B. Gray, California Institute of Technology, Pasadena, CA, and approved October 30, 2006 (received for review September 8, 2006)

We have coupled hybrid quantum mechanics (density functional theory; Car–Parrinello)/molecular mechanics molecular dynamics simulations to a grand-canonical scheme, to calculate the *in situ* redox potential of the $Cu^{2+} + e^- \rightarrow Cu^+$ half reaction in azurin from *Pseudomonas aeruginosa*. An accurate description at atomistic level of the environment surrounding the metal-binding site and finite-temperature fluctuations of the protein structure are both essential for a correct quantitative description of the electronic properties of this system. We report a redox potential shift with respect to copper in water of 0.2 eV (experimental 0.16 eV) and a reorganization free energy $\lambda = 0.76$ eV (experimental 0.6–0.8 eV). The electrostatic field of the protein plays a crucial role in fine tuning the redox potential and determining the structure of the solvent. The inner-sphere contribution to the reorganization energy is negligible. The overall small value is mainly due to solvent rearrangement at the protein surface.

density functional theory | electron transfer | molecular dynamics | reorganization energy

Electron transfer (ET) processes are ubiquitous chemical reactions that occur in a variety of essential biological functions, such as immune response, respiration, and photosynthesis (1–10). Among the different families of ET proteins, single-copper cupredoxins, also known as blue copper proteins, are particularly appealing for theoretical studies because of their relatively small size and the great availability of experimental measurements in the literature. Blue copper proteins exchange electrons among themselves or with other redox proteins, such as cytochrome c551 or nitrite reductase, using a protein-bound Cu metal ion, that can exist in the Cu(II) or Cu(I) redox states (11, 12). The copper ion forms a type 1 Cu-binding site (Fig. 1), which is characterized by a bright blue color, a narrow hyperfine splitting in the electron paramagnetic resonance (EPR) spectra, a high reduction potential (13–15), and a strong structural similarity between oxidized and reduced states (13–17). In fact, in both oxidation states, the copper ion is coordinated by a cysteine (Cys) thiolate group and two histidine (His) nitrogen atoms in a trigonal planar conformation. The coordination polyhedron is completed by one axial ligand, typically a methionine (Met) thioether group. In azurin, a backbone amide oxygen of a glycine (Gly) constitutes an additional axial ligand (18). The structural similarity between the two redox states provides an advantage for the functionality of these ET proteins, as the reorganization free energy (λ) for the redox process is small [0.6–0.8 eV (17, 19)], allowing a high ET rate (20–23). This is not the case for solvated copper ions and synthetic Cu complexes, which tend to have large structural changes concurrent with any variation in their oxidation state (24). The origin of the low value of λ is still unclear. The initial hypothesis implied that the rigidity of the protein would force Cu(II) to be bound in a geometry closer to that preferred by Cu(I) [entatic state and rack theories (25, 26)]. However, this theory has been subject of debate. Quantum chemistry studies on gas phase cluster models (27–30) have proposed that the binding-site geometry is stable for both oxidation states and that the strain imposed by the protein is low and comparable with that found in other metalloenzymes, e.g., alcohol dehydrogenase (24, 28). These studies have also claimed that the increase in redox potential with respect to the solvated ion could be explained, at least qualitatively, in terms of ligand field properties only, and that the active-site contribution to the reorganization free energy (inner-sphere reorganization energy, λ_{inn}) accounts for almost the whole λ. According to these findings, the outer-sphere reorganization energy (λ_{out}), that is, contributions from the protein and the solvent, would not play any major role (24, 27). However, this idea has a few weak points. First, recent dielectric-embedded cluster model-based estimates of azurin–azurin self ET (31) have suggested that, although reduced with respect to the species in water (32), λ_{out} should have at least comparable contributions with respect to λ_{inn} to the total λ. Second, theoretical evidence suggests that the active site might be rather flexible and allows fluctuations of the ligands (24, 28); therefore, finite temperature effects should not be neglected for a correct description of the binding-site properties. Moreover, electron spin echo envelope modulation (ESEEM) measurements (34) have provided evidence that a correct description of the electron spin-density in the oxidized state can only be obtained by explicitly considering larger models than those made by only the Cu ion and its immediate ligands, which are usually used in cluster calculations. Cyclic voltammetry measurements (35–37), which have found that the redox potential of unfolded azurin is 0.1–0.2 eV higher than that of the folded protein, necessarily imply a direct relationship between the protein scaffold and the electronic properties of the copper-binding site. In fact, a direct coupling between the protein dipolar field and its redox properties has been proposed by Warshel and coworkers (38) for plastocyanin and rusticyanin, and we have found a direct effect of the protein electrostatic potential on the optical spectrum of oxidized azurin (data not shown). Finally, recent works pointed out the extreme importance of thermal fluctuations in the ET process (39, 40).

In the present work, we have investigated the Cu(II)/Cu(I) half-reaction in azurin from *Pseudomonas aeruginosa* (18) by means of hybrid quantum mechanics/molecular mechanics (QM/MM) grand canonical molecular dynamics (MD) simulations (41–43). Our calculations are able to reproduce the redox shift reported by experiments and have confirmed the importance of the protein's long-range electrostatic potential for this kind of redox systems (38). We have also found that, if thermal effects are explicitly taken into account, the reorganization free energy

Author contributions: I.T., P.C., and U.R. designed research; M.C. and A.M. performed research; M.C., A.M., and I.T. analyzed data; and M.C. and U.R. wrote the paper.

The authors declare no conflict of interest.

This article is a PNAS direct submission.

Freely available online through the PNAS open access option.

Abbreviations: ET, electron transfer; MD, molecular dynamics; QM/MM, quantum mechanics/molecular mechanics.

§To whom correspondence should be addressed. E-mail: ursula.roethlisberger@epfl.ch.

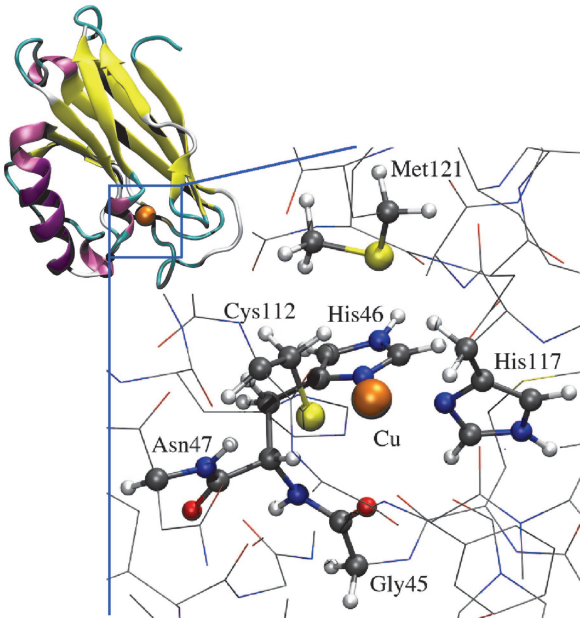

Fig. 1. Structure of azurin. Shown is a cartoon of the protein with the representations and colors assigned according to the secondary structure elements (18). The zoom shows the copper-binding site. The atoms treated at the QM level in our QM/MM calculations are represented by balls and sticks.

is essentially determined by solvent rearrangement around the protein, while the inner-sphere contribution is negligible.

Results and Discussion

The virtual energy gap $\Delta E_{O/R}$ between the two redox states was sampled throughout the 8-ps grand-canonical MD run, and the probability distributions relative to each state are reported in Fig. 2. Despite the relatively limited sampling, the two distributions are comparable, as the width of the fluctuations of the energy gap is rather independent of the oxidation state. Therefore, the standard linear response extrapolation of the redox potential accounts well for the Cu(II)/Cu(I) redox couple in azurin. The inversion of the distributions, plotted at zero driving force condition ($\mu = -\Delta A$), leads to the diabatic free energy curves (presented in Fig. 2). The parabolic fit (44, 45), overall, is good. Deviations found around the equilibrium position of the Cu^{2+} curve might be related to the short sampling duration. The diabatic free energy plot reports an activation free energy of $\Delta A^{\ddagger} = 0.22$ eV for the redox process.

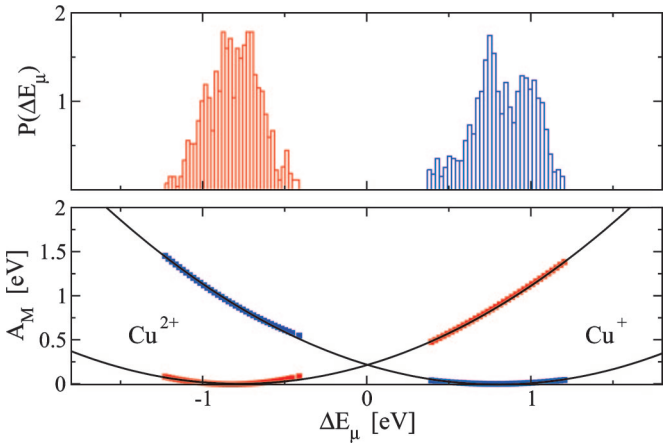

Fig. 2. Diabatic free energy surfaces. (*Upper*) Equilibrium distribution of the ET energy ΔE_{μ} for Cu(I) and Cu(II), given at $\mu = -\Delta A$. (*Lower*) Diabatic free energy profiles constructed from the equilibrium distributions (lower sections, in squares) in the linear response approximation. The upper sections of the free energy profiles (in squares) are obtained by the linear free energy relation. Both sections of data were used to fit the theoretical parabolae (solid lines).

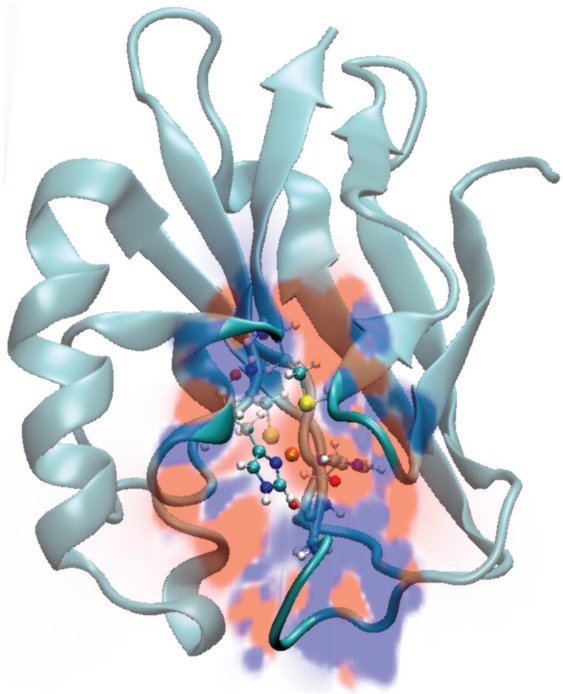

Fig. 3. Electrostatic potential of azurin. The electrostatic potential of the protein scaffold in the metal-binding site is plotted in a red–white–blue scale (red, negative potential; blue, positive potential). Shown is a cartoon of the protein with the active-site atoms represented by balls and sticks.

Redox Potential. The semicouple redox potential for the $Cu^{2+} + e^{-} \rightarrow Cu^{+}$ half-reaction in azurin is obtained by the grand-canonical titration, assuming that the center of the hysteresis is the best estimate of the mid-point chemical potential value (46). Because the redox potential is a relative value, we must compare our result with some reference data. Here, we consider the half reaction of silver ions in water, namely, Ag^{2+}/Ag^{+} (45, 46), as a reference system. These aquo-ion complexes are very similar in both oxidation states, and therefore their reorganization energy is low. Thus, good accurate numerical convergence can be achieved within standard MD simulation sampling (45, 46). Our calculated redox potential $\Delta E^{0}_{Ag^{2+}/Ag^{+}//Cu^{2+}/Cu^{+}} = 1.55$ eV is in very good agreement with the experimental value of 1.63 eV and reproduces the correct redox shift of ≈0.2 eV toward stabilization of the reduced species with respect to Cu ions in water.

As mentioned in the Introduction, the effects of the protein environment on copper redox properties in azurin have been discussed in the literature. Although the increase in the redox potential may be accounted to the specific ligand field that surrounds the metal ion, the importance of long-range effects of the protein frame have not yet been clarified. In particular, the electrostatic field of the protein influences directly the electronic properties of the metal-binding site of blue copper proteins (38). In azurin, the ≈20-Å-long Ala-53–Ser-66 α-helix, which is ≈10 Å away from the copper-binding site, induces a dipolar electrostatic field that is approximately parallel to the direction of the axial ligands (Fig. 3). We qualitatively analyzed the effect of the

Table 1. Cu-binding-site fluctuations

Bond	$\langle d \rangle_{Cu(II)}$, Å	$\langle d \rangle_{Cu(I)}$, Å
Cu-S_{Met121}	3.32 ± 0.28	3.25 ± 0.34
Cu-O_{Gly45}	3.20 ± 0.22	3.15 ± 0.22
Cu-S_{Cys112}	2.13 ± 0.04	2.13 ± 0.06
Cu-N_{His46}	1.98 ± 0.06	1.98 ± 0.08
Cu-N_{His117}	1.99 ± 0.05	1.99 ± 0.09

Shown are average values for distances between the copper ion and its ligands during QM/MM MD runs, for both Cu(I) and Cu(II) oxidation states.

α-helix-induced electrostatic field to the redox potential by repeating single-point QM/MM calculations on configurations coming from our QM/MM MD runs for both redox states, simultaneously nullifying the effect of the electrostatic field of the helix (i.e., setting the MM atom charges to zero). Neglecting the electrostatic field of the helix leads to a substantial increase (0.3 ± 0.1 eV) of the average energy gap between the reduced and oxidized states. This is consistent with the fact that the electrostatic potential at the copper site is negative (Fig. 3) and therefore stabilizes the more positively charged Cu(II) ion. This fold-induced electrostatic stabilization of the Cu(II) state with respect to Cu(I) evidences a subtle mechanism of fine-tuning of the redox properties of blue copper proteins (38). Moreover, it provides a possible explanation for the experimental evidence that oxidized azurin is less prone to unfolding. Under the hypothesis that the major binding-site structural features are not altered upon unfolding, this also accounts for the higher reduction potential of unfolded azurin (35–37).

Reorganization Free Energy. The experimental estimate of the reorganization energy λ = 0.6–0.8 eV (17, 19) is much smaller than that of copper aquo-ions (2.1 eV) (46). The physical basis of this disparity has been addressed in the literature by many propositions, none of them finding a widespread consensus (see Introduction). In particular, it is still debated whether the reorganization energy depends mainly on the copper ion and its ligands (inner sphere, λ_{inn}) or whether it is dominated by the protein and solvent rearrangements (outer sphere, λ_{out}).

Our calculations predict a reorganization free energy of λ = 0.76 eV. The agreement with experiments, along with the correspondence between our calculated and experimental redox potential, supports the reliability of our subsequent estimates of λ_{inn} and λ_{out}, which are not experimentally available.

Our calculated value of $\lambda_{inn} \approx 0.1 \pm 0.06$ eV indicates that the inner-sphere contribution to the overall reorganization free energy is clearly of minor importance. A rationale for this fact is suggested upon closer inspection of the QM/MM simulation data. During dynamics at 300 K, the copper site is rather flexible, and its geometrical fluctuations turn out to be almost identical for both oxidation states (see Table 1). This suggests that, at room conditions, the two species visit essentially the same conformational space, and therefore any redox event would have a negligible λ_{inn} contribution. This result contrasts with findings from static quantum-chemistry calculations (24, 28), which suggested that subtle changes in the structure of the copper ligands (typically of ≈0.05 Å for the planar ligands and 0.2–0.3 Å for the axial ones[¶]) sufficiently justified the energy cost for the redox reaction. Our results propose that 0-K predictions lead to overestimation of λ_{inn}, since they account only for enthalpic contributions and neglect relevant entropic effects.

Because λ_{inn} is small, the largest contribution to λ should originate from outer-sphere contributions of the system. In our simulations, the overall protein structure is not affected by the change in oxidation state of the copper ion (overall rmsd ≈0.35 Å between oxidized and reduced forms), consistent with the corresponding x-ray structures (17). Rather, the solvent rearranges significantly in a region close to the copper ion, specifically, around the copper bound His-117 residue, leading to a $\lambda_{out}^{water} = 0.6 \pm 0.05$ eV. Thus, the water rearrangement upon change of oxidation states accounts for ≈80% of our calculated value of λ. The change in the water structure upon copper reduction was monitored by computing the radial distribution functions with respect to Cu. The side chain of His-117 is bound to Cu by its N_δ atom, and it is in direct contact with the solvent through the N_ε-H side of the imidazole ring (47). The first peak of the Cu-oxygen radial distribution functions (Fig. 4 *Insets*) corresponds to the water molecule that is H-bonded to His-117.

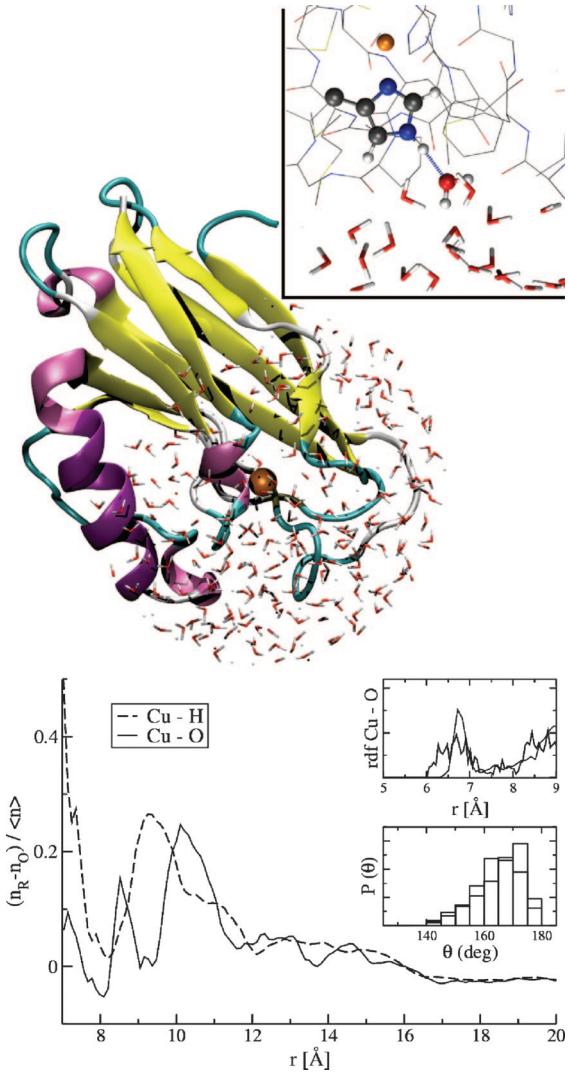

Fig. 4. Solvation properties of azurin. (*Upper*) Solvent exposure of the Cu-binding site. The copper ion, the imidazole ring of His-117, and the closest H-bonded water molecule are represented by balls and sticks. Water molecules within 10 Å of the Cu ion are drawn in licorice, and other heavy atoms of the protein are sketched in lines. (*Lower*) Percentual difference between the coordination number of water molecules around Cu in its two redox states, weighted by the average number of water molecules [defined as $1/2(n_R + n_O)$]. (*Upper Inset*) Cu-O radial distribution functions [black line, Cu(I); red line, Cu(II)]. (*Lower Inset*) Angular distribution of the H-bond between His-117 and the oxygen of the hydrating water molecule, for Cu(I) (black) and Cu(II) (red line).

[¶]These values are typically within one σ of the average of the equilibrium distribution position in our 300-K QM/MM simulations.

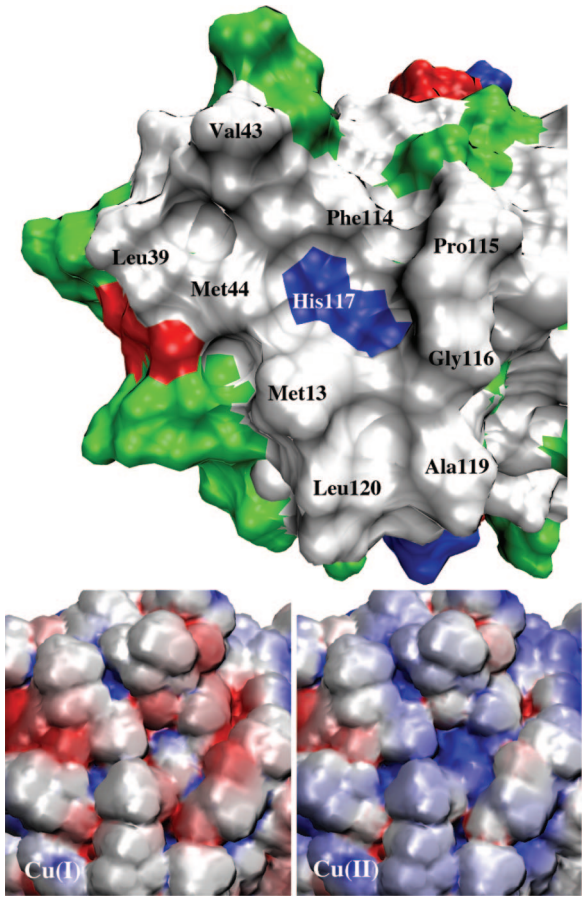

Fig. 5. Electrostatic properties of the surface of azurin. (*Upper*) Protein surface next to His-117 is colored according to solvation properties of the residues (white, hydrophobic; green, polar; blue, basic; red, acidic). (*Lower*) The same surface is colored according to the protein electrostatic potential [from red (negative) to blue (positive)], for Cu(I) and Cu(II) redox states (*Left* and *Right*, respectively).

The radial distribution function for Cu(II) shows a sharp peak around 6.7 Å, whereas the peak associated with Cu(I) is broader. The difference in shape between these peaks can be related to a stronger polarization of the N-H bond for Cu(II). The increased polarization favors a linear geometry for the N-H···O hydrogen bond, consistent with the angular distribution of this H-bond, also reported in Fig. 4, together with the difference in the corresponding coordination numbers for the two redox states. The differential plots indicate a clear rearrangement of the water molecules comprised between 9 and 16.5 Å from the metal ion. This layer corresponds to the first and second solvation shells surrounding the loop region of the azurin protein, and involves a total of ≈260 water molecules. These results agree with experiments on electron tunneling in azurin crystals (48), which suggested that the major contribution to λ comes from hydration water molecules, while bulk water should be of lesser importance. The solvent-exposed residues that surround His-117 are, peculiarly, all hydrophobic (Fig. 5). Because of the reduced presence of H-bonding sites, the structure of the water molecules that wet this portion of the protein surface are rather affected by the long-range electrostatic field of the protein and, in particular, by the oxidation state of the Cu ion <10 Å away. Fig. 5 shows the electrostatic potential at the solvent-accessible surface of azurin for the two oxidation states of copper, computed by solving the linearized Poisson–Boltzmann equation at physiological condition with the APBS program (49). The change in the oxidation state of copper is reflected by strong modification of the electrostatic potential at the protein surface around His-117. In fact, when the copper ion is in the Cu(II) state, its binding site has an overall +1 charge, which is enough to weakly polarize the hydrophobic solvent-exposed region. This is not the case when the copper ion is in its reduced Cu(I) state; this portion of protein surface, in the absence of a nearby net charge, becomes overall more hydrophobic, and in a few sites the potential even inverts its sign. The increase of the hydrophobic character of the protein surface next to His-117 is also responsible for a rearrangement of the solvent-exposed side chains. In particular, the average distance between the sulfur atoms of Met-44 and Met-13, the side chains of which screen the metal site from the solvent, changes from 5.2 to 4.7 Å upon reduction. The rearrangement of the hydrophobic residues and the reduced intensity of the electrostatic potential at the protein surface are therefore the major causes of the rearrangement of the water molecules in the solvation shell of the protein.

Concluding Remarks

Our calculations unveil the crucial effects of the protein environment and solvent for the electronic and structural properties of the Cu(II)/Cu(I) redox reaction in azurin. The spread of the statistical distribution of the energy gap between the reduced and the oxidized states is comparable in both copper oxidation states. This means that the linear response approximation for the environment of the redox event, as hypothesized by Marcus and Sutin (20), accounts well for this system. Our results report a positive shift of ≈0.2 eV with respect to the Cu(II)/Cu(I) couple in water. The redox potential increase, which is ascribed to the peculiar geometry of the copper ligands, is partially damped by the long-range electrostatic potential of the protein. In particular, the dipolar field produced by the Ala-53–Ser-66 α-helix stabilizes Cu(II) more than Cu(I). This is consistent with both the increased stability of the oxidized azurin structure and the increase in the redox potential of Cu bound to defolded azurin (35–37). This also provides evidence for a fine modulation mechanism of redox potentials via electrostatic coupling between the protein frame and the metal-binding site.

The average value of the calculated reorganization free energy, $\lambda = 0.76$ eV, is also in very good agreement with experimental results (17, 19). At 300 K, the metal-binding site is rather flexible, and it does not rearrange significantly upon change of Cu oxidation state. This result is in agreement with previous cluster calculations (24, 27, 28), which did not detect any major strain in the copper ligand structure. Because thermal fluctuations are sufficient to superimpose oxidized and reduced structures of the active site, the inner-sphere contribution to the reorganization energy is negligible. This contrasts static cluster calculations (24, 27, 28), which do not include entropic contributions to λ. Our simulations show that inclusion of thermal effects is crucial to any model that aims at understanding characteristic properties of azurin. The outer-sphere reorganization energy is governed by the protein surface–water interface in the region surrounding His-117. The electrostatic potential of this region, characterized by solvent-exposed hydrophobic side chains, is strongly affected by changes in the oxidation state of the copper ion. This leads to a rearrangement of a shell of ≈260 water molecules, as well as a closer packing of the protein surface residues, upon copper reduction. The distribution of water found for the two copper redox states can also relate to the protein function, as it has been recently proposed that inter-protein ET can occur through structured water layers (10, 50, 51).

Computational Methods

Simulation Details. In our computational setup, the azurin protein was solvated by 8,648 water molecules in a 69 × 61 × 67-Å^3

periodic box. The copper ion [in the oxidized Cu(II) state], its ligands and the backbone of Asn-47, which is H-bonded to the sulfur atom of Cys-112, were described at the spin-polarized DFT level with the Perdew–Burke–Ernzerhof exchange-correlation functional (52) (see Fig. 1). Inclusion of the Asn-47 backbone in the quantum part is fundamental for a correct description of the electronic properties of the metal-binding site and, thus, for a correct determination of the redox potential (53). The rest of the system was treated at the classical mechanics level by the Amber force field [parm98 (54)]. Core-valence interactions were integrated out via norm-conserving Martins–Troullier pseudopotentials (55); the electronic wavefunctions were expanded in plane-waves up to a cutoff of 70 Ry. Integration of the nonlocal parts of the pseudopotential was obtained via the Kleinman–Bylander scheme (56) for all of the atoms except copper, for which a Gauss–Hermite numerical integration scheme was used. The interaction between the classical and quantum parts was described by a fully Hamiltonian hierarchical coupling scheme (42, 57). This setup is able to reproduce the characteristic ground- and excited-state properties of oxidized azurin.

Redox Potentials. The diabatic free energy A_M of the $Cu^{2+} + e^- \rightarrow Cu^+$ semireaction (related to the redox potential $\Delta E^0 = -nF\Delta A$) is defined as

$$\Delta A_M(\Delta E_\mu) = -k_B T \ln p_M(\Delta E_\mu) + \text{const}, \quad [1]$$

where M denotes the oxidized or reduced state, p_M is the probability distribution of the corresponding vertical energy gap ΔE_μ, which is a function of the coordinates of the system $\Delta E_\mu = \Delta E_\mu(\mathbf{R})$. The vertical energy gap ΔE_μ is defined as

$$\Delta E_\mu = \Delta E_0 + \mu, \quad [2]$$

where ΔE_0 is the vertical ionization energy and the constant μ is the electronic chemical potential. In the linear response approximation (20, 45, 46), where the distributions p_M of Eq. **1** are assumed to be Gaussian and equal for both oxidation states, it follows that the free energy difference (and thus, the redox potential) is simply

$$\Delta A = \Delta A^{LR} = \frac{1}{2}(\langle \Delta E_0 \rangle_O + \langle \Delta E_0 \rangle_R) \quad [3]$$

and the reorganization free energy is

$$\lambda = \frac{1}{2}(\langle \Delta E_0 \rangle_O - \langle \Delta E_0 \rangle_R), \quad [4]$$

where $\langle . \rangle_O$ and $\langle . \rangle_R$ represent averages over the MD runs in the oxidized and reduced states, respectively. In our simulations, the redox potential was estimated by running MD in one oxidation state and varying μ until, at a value $\mu = \mu_1$, ΔE_μ became zero. When ΔE_μ crosses zero, MD was run in the other redox state. After some relaxation time, the reaction was induced back by varying μ in the opposite direction as before, up to $\mu = \mu_2$ for which ΔE_μ is zero again. In the linear approximation, the value $\mu_{1/2} = (\mu_1 + \mu_2)/2$ corresponds to the redox potential (46). The inner-sphere contribution to λ was estimated by computing the quantity given in Eq. **1**, by using only the energy of the quantum part to evaluate the gap ΔE_0. The outer-sphere contribution to λ was estimated as proposed by Blumberger and Klein (58), by evaluating ΔE_0 of Eq. **1** as the charge-dipole interactions between the D-RESP charges of the quantum part and the point-charges of the single residues of the protein and the solvent.

More details on the theory and its implementation in the CPMD code used here (33) can be found elsewhere (45, 46).

Computations were done at IDRIS (Paris, France) within the Distributed European Infrastructure for Supercomputing Applications project, and on the IBM Blue Gene machine at Ecole Polytechnique Fédérale de Lausanne. We thank Dr. Jochen Blumberger for constructive discussions and Dr. J. Samuel Arey for comments on the manuscript.

1. Berg JM, Stryer L, Tymoczko JL (2002) *Biochemistry* (Freeman, New York), 5th Ed.
2. Warshel A (1982) *J Phys Chem* 86:2218–2224.
3. Wang JK, Warshel A (1987) *J Am Chem Soc* 109:715–720.
4. Warshel A, Chu ZT, Parson WW (1989) *Science* 246:112–116.
5. Kuharski RA, Bader JS, Chandler D, Sprik M, Klein ML, Impey RW (1988) *J Chem Phys* 89:3248–3257.
6. McLendon G, Hake R (1992) *Chem Rev* 92:481–490.
7. Osyczka A, Moser CC, Daldal F, Dutton PL (2004) *Nature* 427:607–612.
8. Tezcan FA, Crane BR, Winkler JR, Gray HB (2001) *Proc Natl Acad Sci USA* 98:5002–5006.
9. Gray HB, Winkler JR (2003) *Q Rev Biophys* 36:341–372.
10. Gray HB, Winkler JR (2005) *Proc Natl Acad Sci USA* 102:3534–3539.
11. Penfield KW, Gewirth AA, Solomon EI (1985) *J Am Chem Soc* 107:4519–4529.
12. Solomon EI, Lowey MD (1993) *Science* 259:1575–1581.
13. Skyes AG (1990) *Adv Inorg Chem* 36:377–408.
14. Adman T (1991) *Adv Protein Chem* 42:145–197.
15. Messerschmidt A (1998) *Struct Bonding* 90:37–68.
16. Shepard WEB, Anderson BF, Lewandoski DA, Norris GE, Backer EN (1990) *J Am Chem Soc* 112:7817–7819.
17. Di Bilio AJ, Hill MG, Bonader N, Karlsson BG, Villahermosa RM, Malmström BG, Winkler JR, Gray HB (1997) *J Am Chem Soc* 119:9921–9922.
18. Nar H, Messerschmidt A, Huber R, van de Kamp M, Canters GW (1991) *J Mol Biol* 221:765–772.
19. Gray HB, Malmström BG, Williams RJP (2000) *J Biol Inorg Chem* 5:551–559.
20. Marcus RA, Sutin N (1985) *Biochim Biophys Acta* 811:265–332.
21. Winkler JR, Gray HB (1992) *Chem Rev* 92:369–379.
22. Gray HB, Winkler JR (1996) *Annu Rev Biochem* 65:537–561.
23. Langen R, Chang IJ, Germanas JP, Richards JH, Winkler JR, Gray HB (1995) *Science* 268:1733–1735.
24. Ryde U, Olsson MHM, Roos BO, DeKerpel JA, Pierloot K (2000) *J Biol Inorg Chem* 5:565–574.
25. Vallee BL, Williams RJP (1968) *Proc Natl Acad Sci USA* 59:498–505.
26. Malmström BG (1994) *Eur J Biochem* 223:207–216.
27. Pierloot K, De Kerpel JOA, Ryde U, Olsson MHM, Roos BO (1998) *J Am Chem Soc* 120:13156–13166.
28. Ryde U, Olsson MHM (2001) *Int J Quantum Chem* 81:335–347.
29. van Gastel M, Coremans JWA, Sommerdijk H, Hemert MC, Groenen EJJ (2002) *J Am Chem Soc* 124:2035–2041.
30. Jaszewski AR, Tabaka K, Jezierska J, Kedzierska J (2001) *Chem Phys Lett* 367:678–689.
31. Corni S (2005) *J Phys Chem B* 109:3423–3430.
32. Simonson T (2002) *Proc Natl Acad Sci USA* 99:6544–6549.
33. CPMD Consortium (2005) CPMD 3.10.0 (Max-Planck-Institut für Festkörperforschung and IBM Zurich Research Laboratory), www.cpmd.org.
34. Coremans JWA, Poluektov OG, Groenen EJJ, Canters GW, Nar H, Messerschmidt A (1997) *J Am Chem Soc* 119:4726–4731.
35. Winkler J, Wittung-Stafshede P, Leckner J, Malmström BG, Gray HB (1997) *Proc Natl Acad Sci USA* 94:4246–4249.
36. Leckner J, Wittung-Stafshede P, Bonander N, Karlsson BG, Malmström BG (1997) *J Biol Inorg Chem* 2:368–371.
37. Wittung-Stafshede P, Hill MG, Gomez E, Di Bilio AJ, Karlsson BG, Leckner J, Winkler JR, Gray HB, Malmström BG (1998) *J Biol Inorg Chem* 3:367–370.
38. Olsson MHM, Hong G, Warshel A (2003) *J Am Chem Soc* 125:5025–5039.
39. Skourtis SS, Balabin IA, Kawatsu T, Beratan DN (2005) *Proc Natl Acad Sci USA* 102:3552–3557.
40. Hoffman BM, Celis LM, Cull DA, Patel AD, Seifert JL, Wheeler KE, Wang J, Yao J, Kurnikov LK, Nocek JM (2005) *Proc Natl Acad Sci USA* 102:3564–3569.
41. Car R, Parrinello M (1985) *Phys Rev Lett* 55:2471–2474.
42. Laio A, Van de Vondele J, Rothlisberger U (2002) *J Chem Phys* 116:6941–6948.
43. Tavernelli I, Vuilleumier R, Sprik M (2002) *Phys Rev Lett* 88:213002.
44. Tachiya M (1989) *J Phys Chem* 93:7050–7052.
45. Blumberger J, Tavernelli I, Klein ML, Sprik M (2006) *J Chem Phys* 124:064507.
46. Blumberger J, Bernasconi L, Tavernelli I, Vuilleumier R, Sprik M (2004) *J Am Chem Soc* 126:3928–3938.
47. Jeuken LJC, van Vliet P, Verbeet MPh, Camba R, McEnvoy JP, Armstrong A, Canters GW (2000) *J Am Chem Soc* 122:12186–12194.

48. Crane BR, Di Bilio AJ, Winkler JR, Gray HB (2001) *J Am Chem Soc* 123:11623–11631.
49. Baker NA, Sept D, Joseph S, Holst MJ, McCammon JA (2001) *Proc Natl Acad Sci USA* 98:10037–10041.
50. van Amsterdam IMC, Ubbink M, Einsle O, Messerschmidt A, Merli A, Cavazzini D, Rossi GL, Canters GW (2002) *Nat Struct Biol* 9:48–52.
51. Lin J, Balbin IA, Beratan DN (2005) *Science* 310:1311–1313.
52. Perdew JP, Burke K, Ernzerhof M (1996) *Phys Rev Lett* 77:3865–3868.
53. Li H, Webb SP, Ivanic J, Jensen JH (2004) *J Am Chem Soc* 126:8010–8019.
54. Cornell WD, Cieplak P, Bayly CI, Gould IR, Caldwell JW, Kollman PA (1995) *J Am Chem Soc* 117:5179–5197.
55. Troullier N, Martins JL (1991) *Phys Rev B* 43:1993–2006.
56. Kleinman L, Bylander DM (1982) *Phys Rev Lett* 48:1425–1428.
57. Laio A, Van de Vondele J, Rothlisberger U (2002) *J Phys Chem B* 106:7300–7307.
58. Blumberger J, Klein ML (2006) *J Am Chem Soc* 128:13854–13867.